AD-A118 298 NAVAL RESEARCH LAB WASHINGTON DC F/G 8/14
A DYNAMIC MODEL FOR THE AURORAL FIELD LINE PLASMA IN THE PRESEN--ETC(U)
JUL 82 H G MITCHELL, P J PALMADESSO NASA-W-14365
UNCLASSIFIED NRL-MR-4840 NL

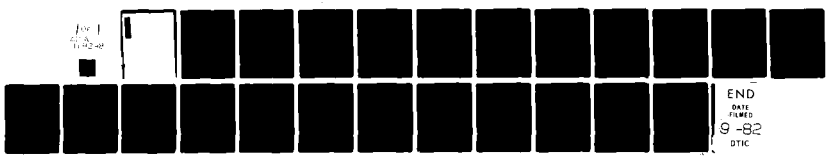

END
DATE FILMED
9-82
DTIC

SECURITY CLASSIFICATION OF THIS PAGE (When Data Entered)

REPORT DOCUMENTATION PAGE		READ INSTRUCTIONS BEFORE COMPLETING FORM
1. REPORT NUMBER NRL Memorandum Report 4840	2. GOVT ACCESSION NO. AD-A118298	3. RECIPIENT'S CATALOG NUMBER
4. TITLE (and Subtitle) A DYNAMIC MODEL FOR THE AURORAL FIELD LINE PLASMA IN THE PRESENCE OF FIELD-ALIGNED CURRENT		5. TYPE OF REPORT & PERIOD COVERED Interim report on a continuing NRL problem. 6. PERFORMING ORG. REPORT NUMBER
7. AUTHOR(s) H.G. Mitchell, Jr. and P.J. Palmadesso		8. CONTRACT OR GRANT NUMBER(s)
9. PERFORMING ORGANIZATION NAME AND ADDRESS Office of Naval Research Arlington, VA 22217 National Aeronautics and Space Admin. Washington, DC 20546		10. PROGRAM ELEMENT, PROJECT, TASK AREA & WORK UNIT NUMBERS 61153N; RR033-02-44; 47-0884-0-2; NASA W-14365
11. CONTROLLING OFFICE NAME AND ADDRESS		12. REPORT DATE July 23, 1982 13. NUMBER OF PAGES 23
14. MONITORING AGENCY NAME & ADDRESS(if different from Controlling Office)		15. SECURITY CLASS. (of this report) UNCLASSIFIED 15a. DECLASSIFICATION/DOWNGRADING SCHEDULE

16. DISTRIBUTION STATEMENT (of this Report)

Approved for public release; distribution unlimited.

17. DISTRIBUTION STATEMENT (of the abstract entered in Block 20, if different from Report)

18. SUPPLEMENTARY NOTES

This work was supported by the Office of Naval Research and by NASA Contract No. W-14365.

19. KEY WORDS (Continue on reverse side if necessary and identify by block number)

Ionosphere-magnetosphere coupling
Auroral field line current
Polar wind

20. ABSTRACT (Continue on reverse side if necessary and identify by block number)

We have developed a dynamic numerical model of the plasma along an auroral field line in order to provide a vehicle for studying ionosphere-magnetosphere coupling processes. The model is a multi-moment multi-fluid approximation of a gyrotropic plasma consisting of three species (electrons, hydrogen ions, oxygen ions) along a segment of auroral magnetic field line extending from an altitude of 800 km to 18 earth radii. We have performed preliminary simulations for the case of a current-free polar wind equilibrium of the field line plasma and the case in which a large upward field-aligned current is applied

(Continues)

DD FORM 1 JAN 73 1473 EDITION OF 1 NOV 65 IS OBSOLETE
S/N 0102-014-6601

SECURITY CLASSIFICATION OF THIS PAGE (When Data Entered)

20. ABSTRACT (Continued)

to the field line. In the former case, the agreement between our model and previous static results is reasonable given the differing boundary conditions inherent in the two cases. In the case of a field-aligned current, we note that the flux tube plasma responds to the current on several time scales. After an initial rapid response due to electron-ion Joule heating, thermal oscillations of the flux tube plasma persist on time scales of the order of one hour, illustrating the complicated nature of the response of a collisionless plasma when heat flow transport is treated in a dynamic manner.

CONTENTS

A DYNAMIC MODEL FOR THE AURORAL FIELD LINE PLASMA IN THE PRESENCE OF FIELD-ALIGNED CURRENT

Introduction

One of the key problems of auroral physics concerns the process by which auroral electrons are accelerated along auroral magnetic field lines. Early theories of the plasma along the field lines above the aurora stated that the collisionless nature of this plasma implied an almost infinite conductivity along the magnetic field so that the field lines could support no parallel electric fields. This conclusion has since been disputed by observational evidence of field-aligned acceleration, first in the "inverted-V" events [reviewed by Frank, 1976] and more directly in the S3-3 satellite data [reviewed by Stern, 1979]. It is now fairly well established that at certain times an anomalously large field is present along auroral field lines at an altitude of several earth radii and is relatively slowly varying in time. This implies the existence of some quasi-steady form of resistivity in the auroral plasma or some other mechanism to maintain a large electric field in a plasma in the absence of collisional resistivity.

A number of mechanisms have been proposed to account for these parallel electric fields. One avenue of research has been devoted to the plasma instabilities which might disrupt the flow of the Birkeland currents parallel to the magnetic field, causing a form of "anomalous" resistivity by wave turbulence. This approach is supported by the observations of terrestrial kilometric radiation emission from this region of the auroral zone [Gurnett, 1974]. Reviews of the theory of plasma instabilities and turbulence in this region can be found in Papadopoulos [1977] and Mozer [1976]. Other mechanisms put forward for auroral acceleration include double layers [Shawhan et al., 1978], electrostatic shocks [Kan, 1975, and Swift, 1975], and magnetic mirror trapping [Lyons, 1980]. However, despite the volume of work which exists on this topic in the form of observation, theory, and numerical simulation, there is no general consensus as to the correct mechanism. One reason for this is the fact that many of these mechanisms are developed and demonstrated for the case of a homogeneous plasma in a constant magnetic field. There are few clear predictions as to their behavior when applied to the auroral plasma. Further, the details of the energy balance are not well understood along the auroral field line even in the absence of current, and these strongly affect the behavior of

Manuscript submitted April 23, 1982.

the particle distributions involved in any resistive mechanism. As a result, it is often hard to say whether a specific process for maintaining the auroral electric field agrees or disagrees with observation.

Clearly, a more global approach to the problem of field line acceleration for the auroral plasma would be useful. The plasma configuration along high latitude field lines has been investigated in the hydrodynamic models of Banks and Holzer [1968] and Schunk and Watkins [1981, 1982] and in the kinetic models of Lemaire and Scherer [1973] and Chiu and Cornwall [1980], among others. These models tend to be static models of steady-state auroral plasma configurations in the absence of an auroral field line current. We will describe in this paper a dynamic model we have been developing for the purpose of understanding the behavior of the auroral field line plasma in the presence of field-aligned current and auroral acceleration mechanisms. This model is a numerical model of a segment of auroral field line beginning in the topside ionosphere and extending well out into the magnetosphere, encompassing the transition of the auroral plasma from collisional to collisionless behavior and employing a multi-moment multi-fluid approximation of the type developed by Schunk [1977]. The details of this model will be given here along with the results of our early simulations of the auroral plasma both with and without field-aligned current. We intend in the future to investigate particular mechanisms of auroral field line acceleration with this model by adjusting the anomalous transport terms in the model's plasma transport equations to simulate the effects of plasma turbulence and by introducing modifications designed to model other proposed acceleration processes. In this way we hope to gain a better understanding of the behavior of these mechanisms in the context of the global behavior of the auroral plasma.

The Field Line Model

The field line model is designed to dynamically simulate the behavior of the plasma in a flux tube encompassing an auroral field line. The field line is assumed to be radial with no curvature and to extend from an altitude of about 800 km in the topside ionosphere out to a distance of 18 earth radii. The actual region of interest in this model is the lower four earth radii or so, the region in which the plasma changes from collisional

to collisionless behavior. The upper region of the flux tube is an extended boundary layer for the purpose of dealing with upper boundary effects. The cross-sectional area of the flux tube diverges as r^3 in the near-earth region, where r is the geocentric distance, and becomes nearly constant in the upper boundary layer. The model is essentially one-dimensional, with all quantities functions of r.

The flux tube plasma consists of three particle species: electrons, hydrogen ions, and oxygen ions. In the present version of the model, the oxygen ions are a static background population at a constant temperature. They are present in the model in order to approximate the behavior of the plasma in the topside ionosphere by providing a thermal reservoir and the correct electron scale height at the lower end of the flux tube. The electrons and hydrogen ions are the dynamic species in the model. The distribution functions for these two species are assumed to be gyrotropic about the field line direction and are characterized by five moments: number density, temperatures parallel and perpendicular to the field line, and species' velocity and heat flow along the field. Including the heat flow as a dynamic quantity rather than calculating it by means of a thermal conduction approximation allows a reasonable treatment of thermal wave effects in the collisionless region of the model.

The moments of the distribution function are treated dynamically using a set of transport equations derived from the 13-moment equations of Schunk [1977]. For a gyrotropic plasma, these equations are:

$$\frac{\partial n_s}{\partial t} = - v_s \frac{\partial n_s}{\partial r} - n_s \frac{\partial v_s}{\partial r} - \frac{n_s v_s}{A} \frac{\partial A}{\partial r} + \frac{\delta n_s}{\delta t} \tag{1}$$

$$\frac{\partial v_s}{\partial t} = - v_s \frac{\partial v_s}{\partial r} - \frac{k}{m_s} \frac{\partial T_{s\parallel}}{\partial r} - \frac{k T_{s\parallel}}{m_s n_s} \frac{\partial n_s}{\partial r} - \frac{k(T_{s\parallel} - T_{s\perp})}{m_s A} \frac{\partial A}{\partial r}$$

$$+ \frac{e_s}{m_s} E - \frac{GM}{r^2} + \frac{\delta v_s}{\delta t} \tag{2}$$

$$k \frac{\partial T_{s\parallel}}{\partial t} = - v_s k \frac{\partial T_{s\parallel}}{\partial r} - 2k T_{s\parallel} \frac{\partial v_s}{\partial r} - \frac{6}{5 n_s} \frac{\partial q_s}{\partial r} - \frac{2}{5} \frac{q_s}{n_s A} \frac{\partial A}{\partial r} + k \frac{\delta T_{s\parallel}}{\delta t} \tag{3}$$

$$k \frac{\partial T_{s\perp}}{\partial t} = - v_s k \frac{\partial T_{s\perp}}{\partial r} - \frac{2}{5n_s} \frac{\partial q_s}{\partial r} - \left(\frac{4}{5} \frac{q_s}{n_s} + v_s k T_{s\perp}\right) \frac{1}{A} \frac{\partial A}{\partial r} + k \frac{\delta T_{s\perp}}{\delta t} \qquad (4)$$

$$\frac{\partial q_s}{\partial t} = - v_s \frac{\partial q_s}{\partial r} - \frac{16}{5} q_s \frac{\partial v_s}{\partial r} - \left(\frac{11}{18} T_{s\parallel} + \frac{8}{9} T_{s\perp}\right) \frac{n_s k^2}{m_s} \frac{\partial T_{s\parallel}}{\partial r}$$

$$- \left(\frac{17}{9} T_{s\parallel} - \frac{8}{9} T_{s\perp}\right) \frac{n_s k^2}{m_s} \frac{\partial T_{s\perp}}{\partial r} + \frac{4k^2}{9m_s} \left(T_{s\parallel} - T_{s\perp}\right)^2 \frac{\partial n_s}{\partial r}$$

$$+ \left[\frac{n_s k^2}{m_s} \left(T_{s\parallel} - T_{s\perp}\right)\left(\frac{1}{3} T_{s\parallel} - \frac{4}{3} T_{s\perp}\right) - \frac{7}{5} v_s q_s\right] \frac{1}{A} \frac{\partial A}{\partial r} + \frac{\delta q_s}{\delta t} \qquad (5)$$

where n_s is the number density, v_s is the velocity, $T_{s\parallel}$ is the parallel temperature, $T_{s\perp}$ is the perpendicular temperature, q_s is the heat flow, m_s is the mass, and e_s is the charge of species s, A is the cross-sectional area of the flux tube, E is the electric field parallel to the field line, k is Boltzmanns' constant, G is the gravitational constant, and M is the mass of the earth. For a given moment F of the distribution function, $\delta F/\delta t$ is the change in F due to resistive and plasma turbulence effects. The present version of the field line model includes only resistivity due to Coulomb collisions among the three particle species in the model. Once the behavior of this simulation is understood for this case, the turbulence terms will be altered to reflect the behavior of the particle distribution functions in the presence of plasma microprocesses. The specific resistive terms used in the present simulation are Burgers' [1979] 'linear' collision terms for the case of Coulomb collisions, given by

$$\frac{\delta n_s}{\delta t} = 0 \qquad (6)$$

$$\frac{\delta v_s}{\delta t} = \sum_t \nu_{st} (v_t - v_s) \qquad (7)$$

$$k \frac{\delta T_{s\parallel}}{\delta t} = \sum_t \frac{m_s \nu_{st}}{(m_s + m_t)} \left[\frac{6}{5} k T_{t\parallel} - \left(2 + \frac{4m_t}{5m_s}\right) k T_{s\parallel} + \frac{4}{5} k T_{t\perp} + \frac{4m_t}{5m_s} k T_{s\perp}\right.$$

$$\left. + \frac{6}{5} m_t (v_t - v_s)^2\right] \qquad (8)$$

$$k\frac{\delta T_{s\perp}}{\delta t} = \sum_t \frac{m_s \nu_{st}}{(m_s+m_t)} \left[\frac{2}{5} kT_{t\parallel} + \frac{2m_t}{5m_s} kT_{s\parallel} + \frac{8}{5} kT_{t\perp} - \left(2 + \frac{2m_t}{5m_s}\right) kT_{s\perp}\right.$$

$$\left. + \frac{2}{5} m_t (v_t - v_s)^2\right] \tag{9}$$

$$\frac{\delta q_s}{\delta t} = \sum_t \frac{n_s m_s \nu_{st}}{(m_s+m_t)^2} \left[\frac{27}{10} m_t \frac{q_t}{n_t} - \left(3m_s + \frac{8}{5} m_t + \frac{13}{10}\frac{m_t^2}{m_s}\right) \frac{q_s}{n_s}\right.$$

$$\left. + \frac{3}{2}\frac{m_t}{m_s}(m_t+m_s) kT_s (v_s - v_t)\right] \tag{10}$$

where each sum includes all charged particles species in the simulation and ν_{st} is the Coulomb collision frequency,

$$\nu_{st} = \frac{(32\pi)^{1/2} e_s^2 e_t^2 n_t}{3m_s^2} \left(1 + \frac{m_s}{m_t}\right) \left(\frac{kT_s}{m_s} + \frac{kT_t}{m_t}\right)^{-3/2} \ln \Lambda \tag{11}$$

($\ln \Lambda$ is the Coulomb logarithm and $T_s = (T_{s\parallel} + 2T_{s\perp})/3$ is the total temperature of species s).

The scale of this model is large compared to the electron Debye length, so the transport equation (1) for electron number density may be replaced by an expression for charge neutrality:

$$n_e = n_p + n_i. \tag{12}$$

(The subscripts e, p, and i represent electrons, hydrogen ions, and oxygen ions respectively.) Further, the assumption will be made that the total flux tube current remains constant at some fixed value I during a simulation, which implies that the electron velocity transport equation (2) is replaced by

$$v_e = \frac{1}{n_e}\left(n_p v_p - \frac{I}{eA}\right). \tag{13}$$

This assumption reflects the fact that the auroral current generator is not strongly affected by the behavior of the flux tube plasma. The assumption of charge neutrality and constant current along the field line allows the parallel electric field E to be calculated from a generalized Ohm's law constructed from the electron and ion velocity transport equations (2):

$$E = \frac{m_s}{en_eA}\frac{\partial}{\partial r}\left(n_pv_p^2A - n_ev_e^2A\right) - \frac{1}{e}\left[\frac{\partial T_{e\parallel}}{\partial r} + \frac{T_{e\parallel}}{n_e}\frac{\partial n_e}{\partial r}\right.$$

$$\left. + \frac{\left(T_{e\parallel}-T_{e\perp}\right)}{A}\frac{\partial A}{\partial r}\right] - \frac{n_im_eGM}{n_eer^2} + \frac{m_e}{e}\left[\frac{\delta v_e}{\delta t} - \frac{n_p}{n_e}\frac{\delta v_p}{\delta t}\right] \qquad (14)$$

where terms on the order of m_e/m_p have been neglected.

The field line model, therefore, uses equations (1)-(5) for hydrogen ions and equations (3)-(5) for electrons to step the values of these distribution moments forward in time, while calculating the electric field and electron density and velocity self-consistently at each time with equations (12)-(14). The simulation calculates transport using the simple partial donor cell method (Hain, 1978) on an unequally spaced grid. The segment of the field line being modelled is divided into about 100 cells. The cell size at the lower end of the segment is small, around 50 km, in order to properly deal with the transport in the presence of the large density gradients due to the small oxygen scale height. The cell size increases with altitude until it reaches roughly 1000 km at an altitude of 6 earth radii (R_E). At this altitude, the upper boundary layer begins, and the cell size begins to increase rapidly, reaching about one R_E at the upper boundary of the model. The time step for this simulation is determined primarily by the transit time of a thermal electron in a cell at the lower end of the field line and is set at about .06 seconds.

Preliminary simulations with the field line model indicated that the behavior of the simulation could become unstable if the species heat flows were allowed to grow too large. A subsequent wave analysis of the model equations (1)-(5) and (12)-(14) revealed that an unstable ion thermal wave exists when the velocity of the ion heat flow exceeds roughly the ion thermal velocity, i.e.,

$$|q_p|/n_pT_p > (kT_p/m_p)^{1/2} \tag{15}$$

This indicates that the thermal velocity is a natural limit on the rate of energy flux relative to the species velocity. The form of a distribution function with a heat flow of this magnitude is highly non-Maxwellian, and it is to be expected that the instability would tend to reduce the heat flow. As a result, the field line model limits the magnitude of the species' heat flow by using the relation

$$|q_s| < n_sT_s(kT_s/m_s)^{1/2} \tag{16}$$

This limit tends to have little or no effect on the electrons because of their large thermal velocity, but can be a relatively stringent condition for hydrogen ions. It slows the response of the hydrogen ion distribution to large temperature gradients, allowing them to persist for longer periods of time.

The Polar Wind Simulation

The first simulations with the field line model were performed to construct a steady-state configuration of the field line plasma in the current-free case. We began by initializing the flux tube in a polar wind configuration similar to that of Banks and Holzer [1968]. In the polar wind, hydrogen ions are accelerated upwards in the flux tube to supersonic velocities due to the flux tube divergence and the small partial pressure of H^+ at the upper end of the field line. The outward H^+ flux depletes the hydrogen ion population at lower altitudes, and, as a result, oxygen ions are the dominant ion species up to an altitude of around 4000 km. The O^+-e charge separation electric field in this region provides the initial H^+ acceleration up the field line. In the model of Banks and Holzer, the population of H^+ is maintained against depletion by O^+-H charge exchange at the altitudes below 1000 km, and the hydrogen ion escape flux is limited to about 6×10^8 $cm^{-2}sec^{-1}$ at 1000 km. In the field line model, there are no neutral species at this point, so the hydrogen ion flux is maintained by a fixed density and upward velocity for H^+ at 800 km, the lower boundary of the model. As a result, the hydrogen ion number density tends to be somewhat greater in the lowest few cells of the field line model than would be expected in the presence of O^+-H charge exchange.

The model of Banks and Holzer assumed that the charged particle species in the flux tube had uniform temperatures and, therefore, heat flow was neglected. We assumed the same, initializing the three flux tube particle species at a constant temperature of 3000 K with no heat flow. To begin our simulations, the transport of temperature and heat flow were suppressed in the field line model in an attempt to duplicate the results of Banks and Holzer. The model achieved a steady-state polar wind under these conditions, with the number density and velocity profiles shown in Fig. 1a,b. Once this equilibrium had been reached, the temperature and heat flow transport were "turned on", and the simulation was run until a new steady-state was achieved. The lower boundary temperature was held fixed at 3000 K during the simulation. This is a somewhat artificial condition, but the actual thermal balance at this altitude involves modelling the upper ionosphere in more detail than this simulation is capable of at the present time. The upper boundary temperature was determined by an outflow condition in that thermal gradients propagating up the field line were allowed to propagate out of the simulation.

The temperature profiles from the new steady-state are shown in Fig. 2. The primary effect displayed by the electron temperatures in this equilibrium is adiabatic cooling due to the expansion of the cross-sectional flux tube area with height. At the lower end of the field line, the high rate of expansion causes rapid cooling, and the resulting temperature gradient is maintained by low thermal conductivity due to high particle density. The electron temperature profiles tend to flatten out near the upper end of the tube as both the rate of expansion and the particle densities decrease. In addition, the electron temperatures exhibit a small anisotropy at the upper end of the tube due to unequal rates of cooling in the perpendicular and parallel directions. This may also be viewed as the fluid model manifestation of the mirror effect, with perpendicular energy being transferred into parallel energy as the electrons are accelerated upwards in the diverging magnetic field.

The hydrogen ion temperatures, on the other hand, increase with increasing altitude at the lower end of the flux tube, before beginning to exhibit adiabatic cooling at an altitude of three-fourths to one R_E. The

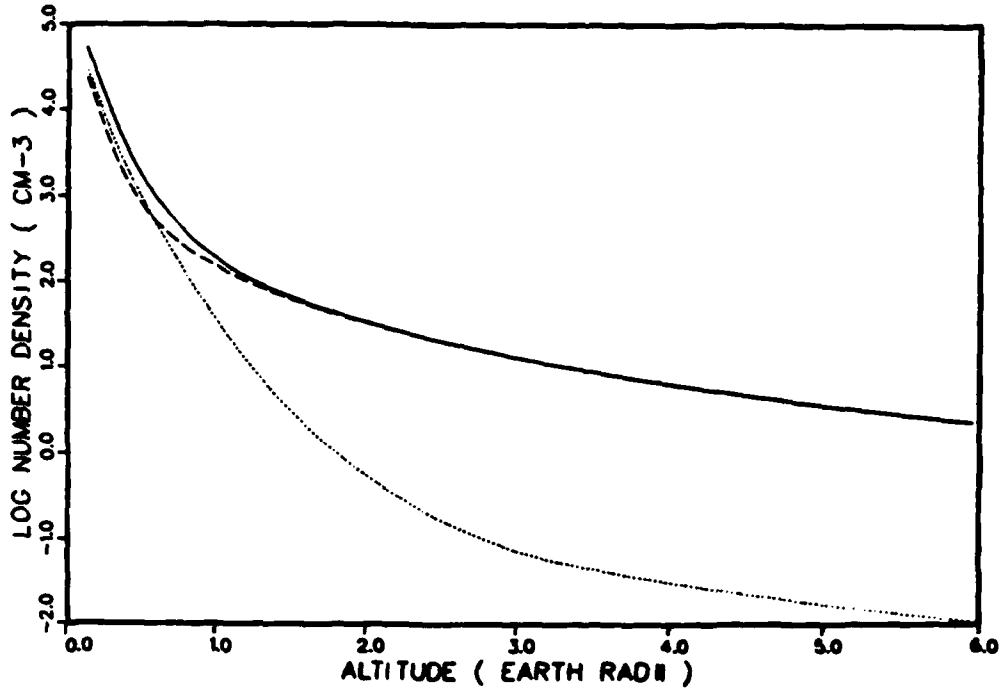

Fig. 1(a) — Number densities for the steady-state polar wind with no field-aligned current: e (solid curve), H^+ (dashed curve), 0^+ (dotted curve).

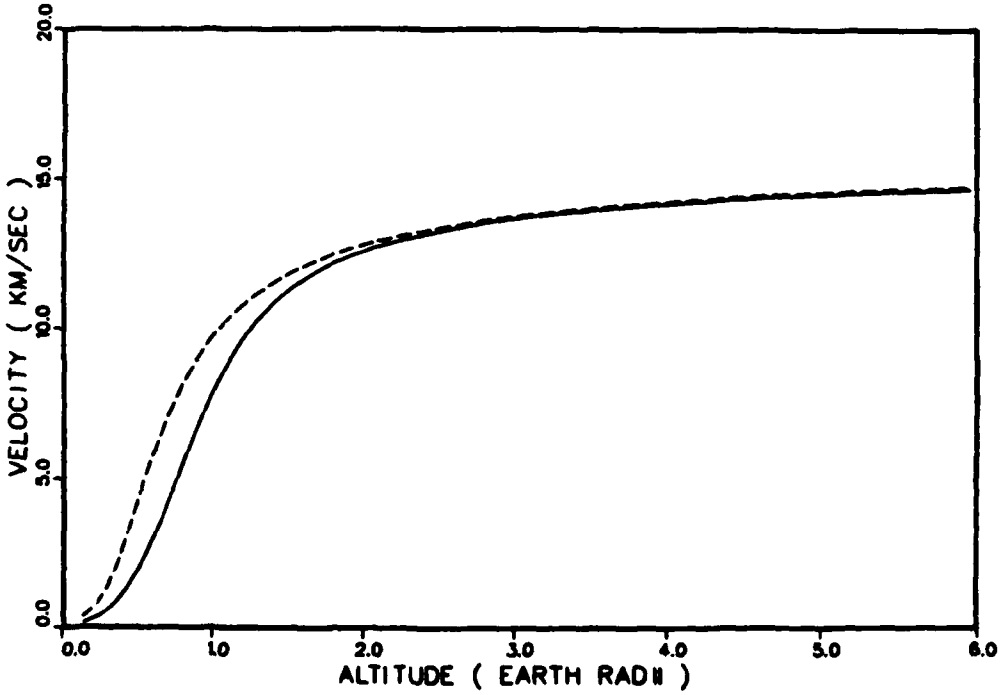

Fig. 1(b) — Velocities for the steady-state polar wind with no field-aligned current: e (solid curve), H^+ (dashed curve). The 0^+ velocity is uniformly zero.

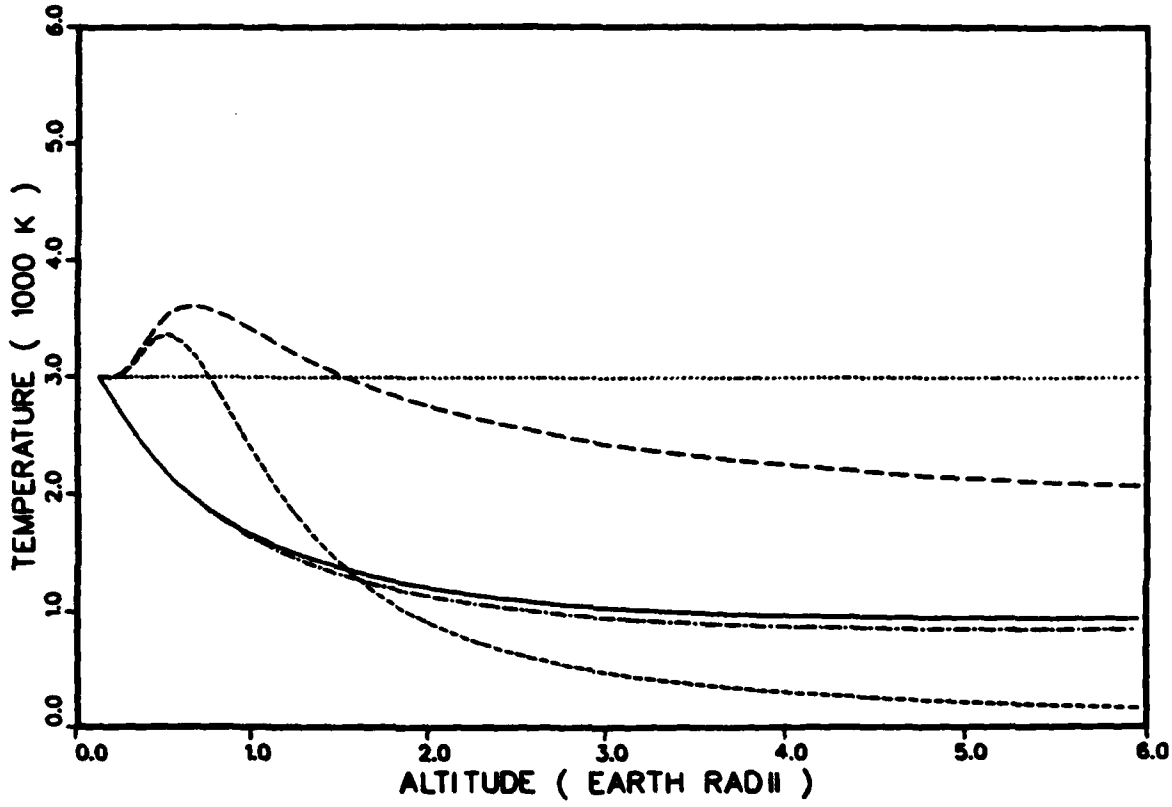

Fig. 2 — Temperatures for the steady-state polar wind with no field-aligned current: $T_{e\parallel}$ (solid curve), $T_{e\perp}$ (dot-dash curve), $T_{H\parallel}$ (long dashed curve), $T_{H\perp}$ (short dashed curve), T_o (dotted curve).

temperature increase is caused by the Joule heating of the hydrogen from collisions with the oxygen ions, a process which heats in the parallel direction more strongly than the perpendicular. The strength of this effect decreases rapidly with altitude due to the small scale height of the oxygen, allowing the adiabatic cooling to become dominant at about 4000 km altitude. The anisotropy of the cooling is much more evident in the hydrogen ions than in the electrons because of the supersonic hydrogen velocities and the fact that, in the collisionless region, heat transport along the field line is less efficient for the hydrogen than for the electrons. As a result, the hydrogen temperature profiles maintain significant gradients at higher altitudes than the electron profiles and exhibit large temperature anisotropies at the upper end of the flux tube.

It is instructive to compare these results with those of Schunk and Watkins [1981, 1982]. These works model current-free steady-state configurations of the auroral field line plasma by integrating up the field line the steady-state form of a set of transport equations for a three species (e, H^+, O^+) plasma similar to the ones in equations (1)-(5). The steady-state configurations which result are a function of the lower boundary (1500 km altitude) conditions, specifically the values of the species' density, velocity, temperature, and temperature gradient. Comparing the results of our simulations with those of Schunk and Watkins [1982] for the hydrogen ion profiles in the case of supersonic polar wind, a number of similarities can be seen. For low electron temperatures, both exhibit an anisotropic hydrogen ion cooling resulting in a larger parallel than perpendicular temperature at the upper end of the field line. Also, both have a region in which the parallel temperature increases with altitude before adiabatic cooling dominates. The rate of cooling for the hydrogen ions is less in our simulation, most likely because both the oxygen ions and the electrons are hotter at the lower end of the field line (3000 K in our simulation vs. 1000 K in that of Schunk and Watkins). The highly anisotropic cooling of the hydrogen ions is also a feature of another steady-state polar wind model, that of Holzer, Fedder, and Banks [1971], which also attempted to realistically deal with the ion heat flow in the collisionless region. The heat flow for hydrogen ions is upward and monotonically decreasing in these models, implying that the polar wind requires an outward flow of heat from the ionosphere. The magnitude of the

heat flow is roughly an order of magnitude greater in our simulation than that of Schunk and Watkins due to the smaller hydrogen ion velocity at the lower end of the field line in our model. A smaller velocity implies a smaller rate of advective heating, forcing a greater heat flow.

The electron profiles of Schunk and Watkins [1981] cannot be directly compared to our simulation results. By assuming a positive electron temperature gradient at an altitude of 1500 km, they achieve an equilibrium in which the electron temperatures are monotonically increasing with altitude and the electron heat flow is down the field line. Further, the temperature anisotropy is reversed in the upper region of the field line, with the perpendicular temperature being the larger. Thus, the positive temperature gradient boundary condition for the electrons forces the upper boundary of the field line to act as a heat source for the flux tube. The outflow condition in our model, on the other hand, treats the upper boundary as an electron heat sink, resulting in a monotonically decreasing electron temperature with altitude. As long as the electron species velocity is less than the electron thermal velocity, the assumed electron temperature of the upper boundary plasma has a strong effect on the electron temperature profiles in the flux tube. The supersonic outflow of hydrogen ions in the polar wind implies that the energy flux must be outward for the hydrogen ions, with the result that only the ionosphere can provide a heat source for H^+ regardless of the assumed temperature of the upper boundary protons. Schunk and Watkins [1982] note that, for subsonic H^+ outflow, the upper boundary plasma can provide a proton heat source.

A Field-Aligned Current Simulation

Preliminary simulations have been performed with the field line model in the presence of current parallel to the magnetic field and we would like to briefly describe one of these simulations. In this case, a constant upward current of 5.4×10^{-6} A/m^2 at an altitude of 800 km was assumed for the duration of the simulation. This value was chosen to illustrate the effect of a large downward electron energy flux on the flux tube plasma. The initial state of the flux tube is assumed to be the steady-state polar wind described in the previous section.

The behavior of the electron temperature profiles for the first ten

minutes after current onset are shown in Fig. 3a,b. Initially, Joule heating due to the relative electron-hydrogen ion drift causes a rapid temperature increase at the lower end of the field line in both the parallel and perpendicular directions. The outward electron heat flow increases in response to the resulting electron temperature gradient, thus heating the electrons at higher altitudes. Note that the gradients are opposite for the perpendicular and parallel temperatures in the 1 to 4 R_E altitude range, an effect caused by the transfer of parallel to perpendicular energy of the precipitating electrons in the converging magnetic field. Also, the upward electron heat flow has an anisotropic effect on the electron temperature, resulting in a cooling of the perpendicular temperature at higher altitudes as energy is transported upward. Eventually, a rough balance is achieved in the collisionless region between upward heat flow and downward convecting electron energy flux. The location and magnitude of the maximum in the parallel temperature profile for this equilibrium is very sensitive to the rate of flux tube divergence in the collisionless region. As the electron temperature rises in the lower end of the flux tube, the hydrogen ions are also collisionally heated in this region, as shown in the hydrogen ion temperature profiles for the first ten minutes in Fig. 4a,b. Thus, a thermal wave propagating up the field line is also created in the parallel hydrogen ion temperature, although a much slower wave due to the smaller ion thermal velocity. The increased electron temperature also results in an increased ambipolar electric field in the lower regions of the flux tube, causing an increased hydrogen ion outflow velocity (Fig. 5).

During the next twenty minutes of the simulation, the hydrogen ion thermal wave generated previously propagates into the upper boundary layer as the temperature of the hydrogen ions continues to increase in the collisional region below 1 R_E altitude due to $e\text{-}H^+$ collisions (Fig. 6). These profiles of the parallel hydrogen ion temperature illustrate the difference between a treatment of heat flow by a thermal conduction approximation and one in which heat flow is a dynamic quantity. In the latter case, the heat flow has a finite response time to thermal gradients. As a result, the flux tube plasma exhibits the large thermal oscillations shown in Fig. 6 rather than having the thermal gradients damped out by the large thermal conductivity of a collisionless plasma. As

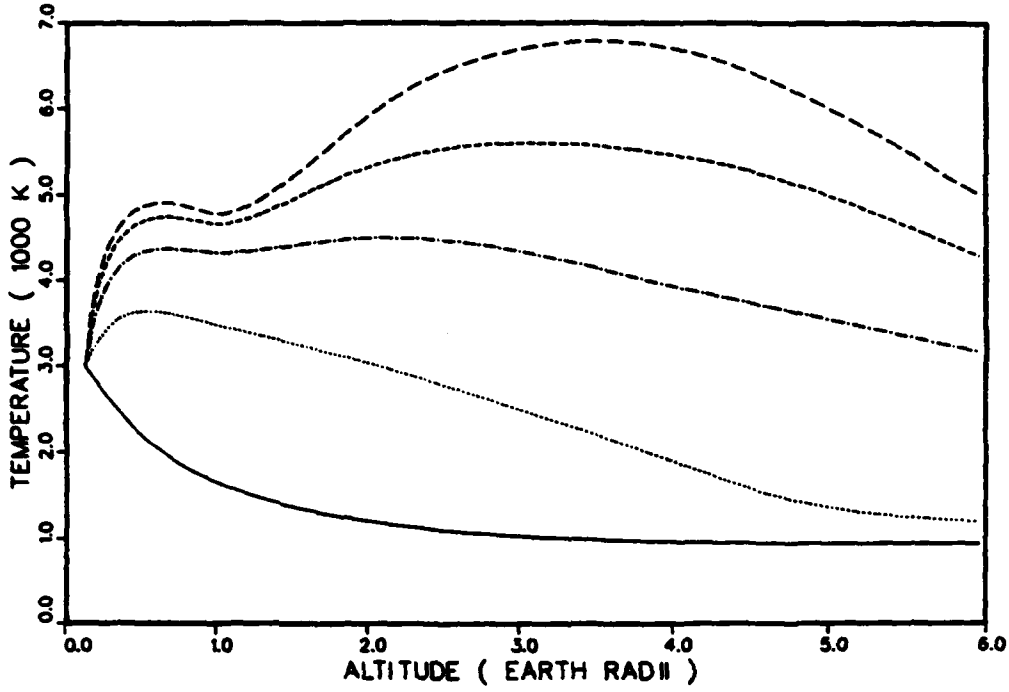

Fig. 3(a) — Parallel electron temperatures for the first ten minutes after the onset of a current of 5.4 $\mu A/m^2$ at 800 km: 0 min (solid curve), 2.5 min (dotted curve), 5 min (dot-dash curve), 7.5 min (short dashed curve), 10 min (long dashed curve).

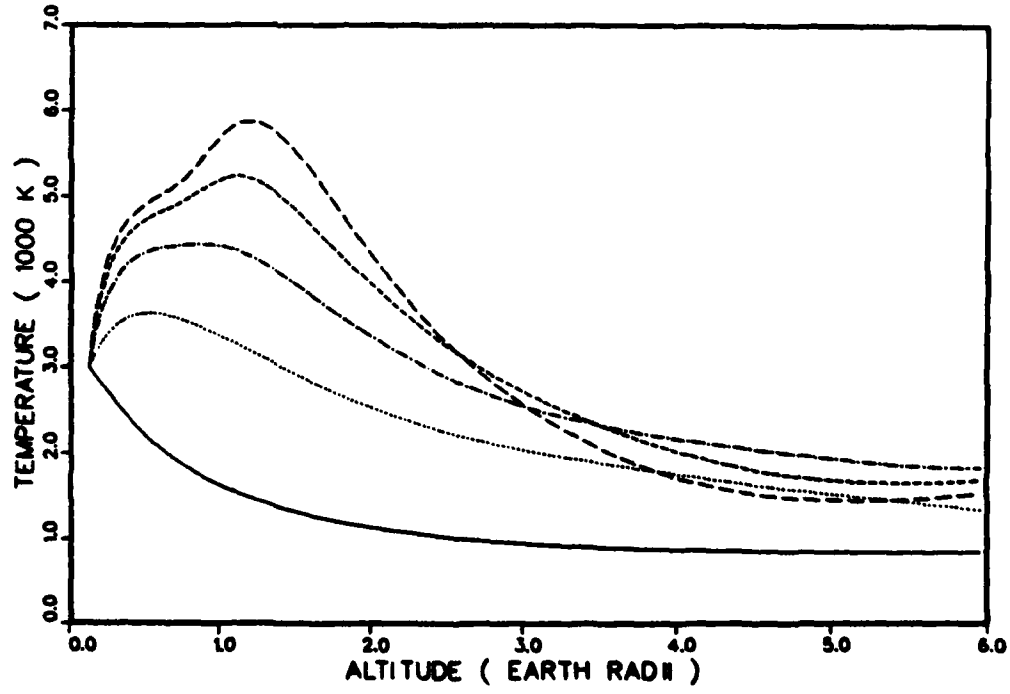

Fig. 3(b) — Perpendicular electron temperatures for the first ten minutes after current onset. (Same legend as Fig. 3a)

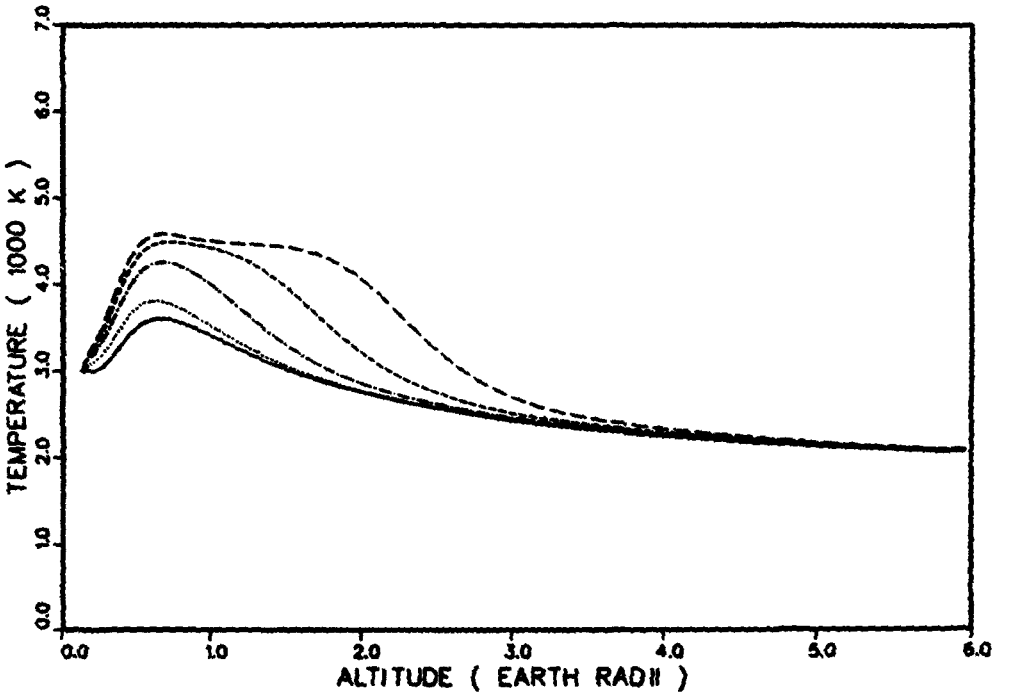

Fig. 4(a) — Parallel hydrogen ion temperatures for the first ten minutes after current onset. (Same legend as Fig. 3a.)

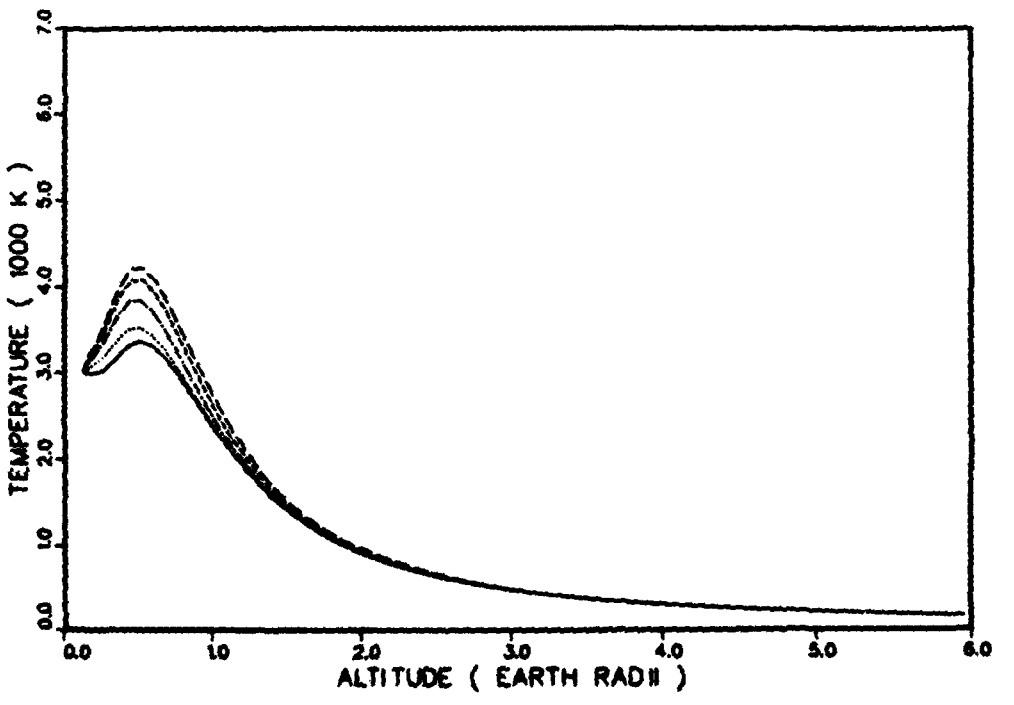

Fig. 4(b) — Perpendicular hydrogen ion temperatures for the first ten minutes after current onset. (Same legend as Fig. 3a.)

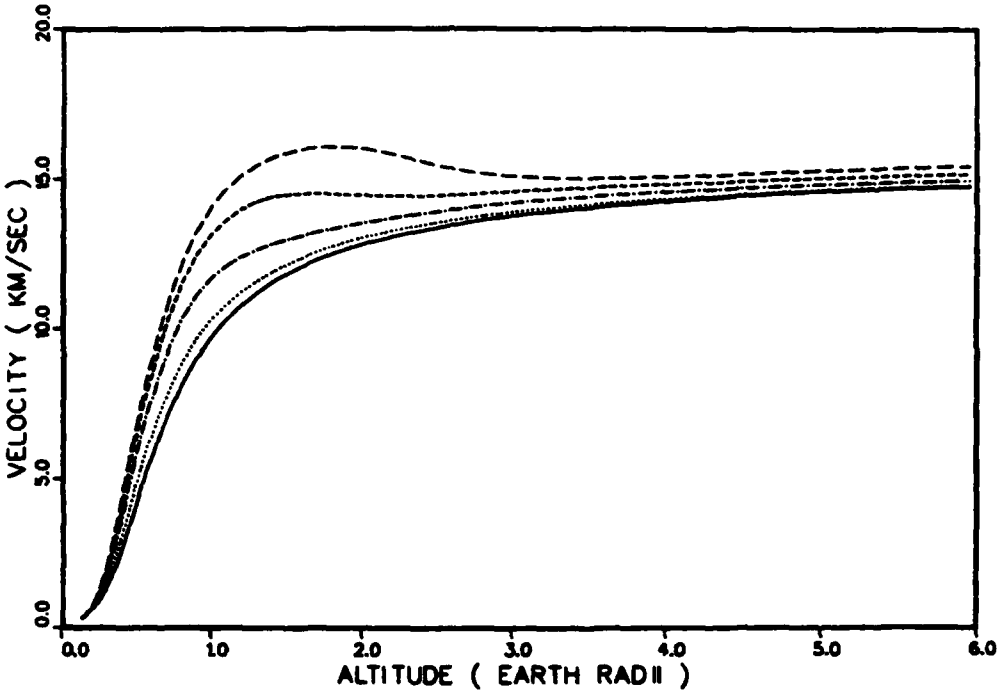

Fig. 5 — Hydrogen ion velocities for the first ten minutes after current onset. (Same legend as Fig. 3a.)

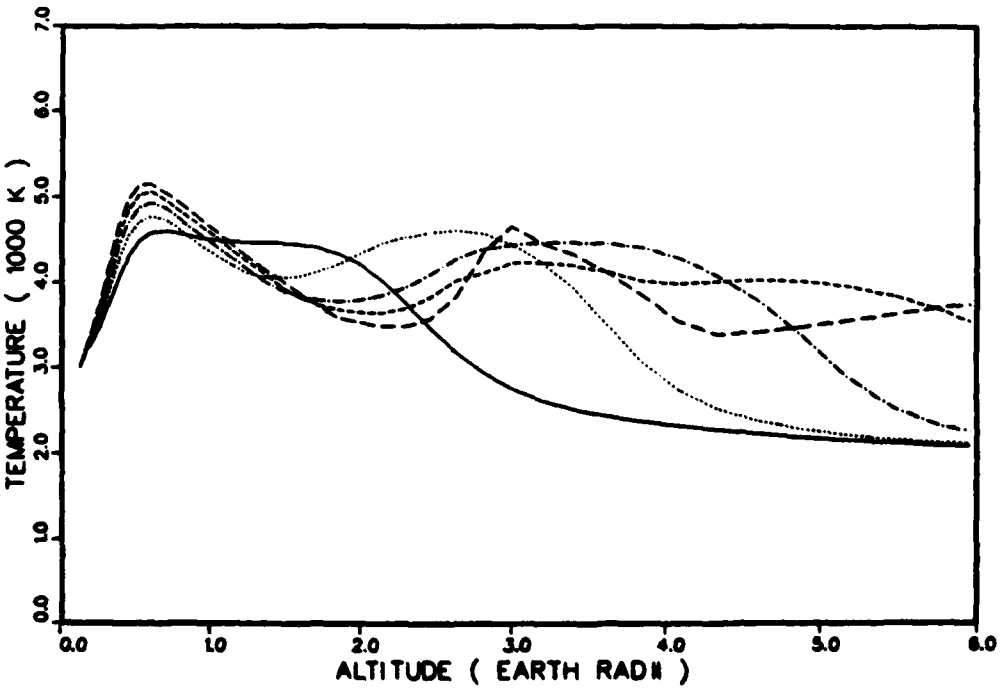

Fig. 6 — Parallel hydrogen ion temperatures for the times from ten minutes to thirty minutes after current onset: 10 min (solid curve), 15 min (dotted curve), 20 min. (dot-dash curve), 25 min. (short dashed curve), 30 min (long dashed curve).

the simulation continues, such thermal oscillations are seen in both the hydrogen ion and electron temperature profiles until, at about one hour into the simulation, the electron thermal waves have propagated through the upper boundary layer and affected the upper boundary cell. At this point the simulation began to exhibit a form of thermal runaway due to the interaction between the precipitation electron distribution and the outward heat flow at the upper boundary, and the simulation was halted. We do not view this failure of the upper boundary condition as a major restriction on the validity of the simulation because the one-dimensional field line plasma and constant current approximations would not be accurate for a simulation which lasted much longer than this.

The point that we wish to stress here is that the flux tube plasma seems to have a rapid initial response to the onset of current, one affecting the electron temperature predominantly. After this response, it is not clear that the plasma "settles down" to some equilibrium configuration in a reasonable time. Large electron and ion thermal waves can persist for relatively long times when the heat flows are treated dynamically. The preliminary nature of our field-aligned current simulations prevents us from describing these results in too much detail. One of our future goals is to use this model to investigte the behavior of these thermal waves for a range of currents and upper boundary layer configurations.

Summary

We have described here some of the preliminary results of our model for the behavior of the auroral field line plasma. Our results for equilibrium in the current-free case are in reasonable agreement with the previous work in this area, illustrating the important role that the upper boundary layer plays in determining the temperature profile of the electron population in constrast to the relative insensitivity of the supersonic hydrogen ion population to this layer. The early simulations with current which we have performed suggest that, although much of the flux tube dynamics depends on the energy transfer among particle species in the collisional regions of the tube, the time scale on which the field line plasma achieves equilibrium is highly dependent on the behavior of the

energy transport in the collisionless region. In fact, there may exist no equilibrium on the field line in the presence of a current varying on the time scale of interest in this problem.

The results presented here are meant to illustrate the kinds of behavior the field line model manifests and to point the way for future improvements in the model. Because of the importance of the collisional regime of the topside ionosphere in the dynamics of the entire field line, one of our first steps will be to investigate the manner in which changes in the details of this regime affect the behavior of the field line simulations. Also, we feel that there is much more to be done in order to understand the effect the upper boundary layer has on the flux tube plasma. It is our intention to proceed in these areas in addition to our main goal, that of investigating the effect of anomalous resistivity and electric field mechanisms in the collisionless region of our model.

Acknowledgement

This work was supported by the Office of Naval Research and by NASA Contract No. W-14365.

References

Banks, P.M., and T.E. Holzer, The polar wind, J. Geophys. Res., 73, 6846-6854, 1968.

Burgers, J.M., Flow Equations for Composite Gases, Academic Press, New York, 1969.

Chiu, Y.T., and J.M. Cornwall, Electrostatic model of a quiet auroral arc, J. Geophys. Res., 85, 543-556, 1980.

Frank, L.A., Hot plasmas in the earth's magnetosphere, in Physics of Solar Planetary Environments, edited by D.J. Williams, pp. 685-700, AGU, Washington, D.C., 1976.

Gurnett, D.A., The earth as a radio source: terrestrial kilometric radiation, J. Geophys. Res., 79, 4227-4238, 1974.

Hain, K., The partial donor cell method, NRL Memorandum Report 3713, Naval Research Laboratory, Washington, D.C., 1978.

Holzer, T.E., J.A. Fedder, and P.M. Banks, A comparison of kinetic and hydrodynamic models of an expanding ion-exosphere, J. Geophys. Res., 76, 2453-2468, 1971.

Kan, J.R., Energization of auroral electrons by electrostatic shock waves, J. Geophys. Res., 80, 2089-2095, 1975.

Lemaire, J., and M. Scherer, Kinetic models of the solar and polar winds, Rev. Geophys. Space Phys., 11, 427-468, 1973.

Lyons, L.R., Generation of large-scale regions of auroral current electric potentials, and precipitation by the divergence of the convection electric field, J. Geophys. Res., 85, 17-24, 1980.

Mozer, F.S., Anomalous resistivity and parallel electric fields, in Magnetospheric Particles and Fields, edited by B.M. McCormac, pp. 125-136, D. Reidel, Dordrecht, Netherlands, 1976.

Papadopoulos, K., A review of anomalous resistivity for the ionosphere, Rev. Geophys. Space Phys., 15, 113-127, 1977.

Schunk, R.W., Mathematical structure of transport equations for multispecies flows, Rev. Geophys. Space Phys., 15, 429-445, 1977.

Schunk, R.W., and D.S. Watkins, Electron temperature anisotropy in the polar wind, J. Geophys. Res., 86, 91-102, 1981.

Schunk, R.W., and D.S. Watkins, Proton temperature anisotropy in the polar wind, J. Geophys. Res., 87, 171-180, 1982.

Shawhan, S.D., C.-G. Falthammar, and L.P. Block, On the nature of large auroral zone electric fields at 1-R_e altitude, J. Geophys. Res., 83, 1049-1054, 1978.

Stern, D.P., The electric field and global electrodynamics of the magnetosphere, Rev. Geophys. Space Phys., 17, 626-640, 1979.

Swift, D.W., On the formation of auroral arcs and the acceleration of auroral electrons, J. Geophys. Res., 80, 2096-2108, 1975.